



Cite this: *Catal. Sci. Technol.*, 2025, 15, 5491

# Support modification by phosphonic acid ligands controls ethylene hydroformylation on single-atom rhodium sites

Zachary W. Meduna,  Daniel K. Schwartz  and J. Will Medlin \*

To investigate the ability of surface-bound ligands to control activity toward ethylene hydroformylation, we modified site-isolated  $\text{Rh}_1/\text{TiO}_2$  with a series of substituted benzyl phosphonic acids. We found that modification of the support by phosphonic acids reduced break-in times for hydroformylation by 4× and increased absolute hydroformylation activity by up to 18× compared to unmodified catalyst at 150 °C. All functionalized catalysts improved hydroformylation activity by at least 9× and improved selectivity by between 7× and 60× relative to the unmodified catalyst. Carbon monoxide probe-molecule spectroscopy indicated that the enhancements in activity among modified samples were due to changes in the local environment of the active Rh site. Specifically, the bite angle of adsorbed carbon monoxide, as determined from infrared spectra, correlated with hydroformylation activity. These findings demonstrate that  $\text{Rh}_1$  active sites are highly sensitive to modification of the support with organic ligands.

Received 7th June 2025,  
Accepted 11th August 2025

DOI: 10.1039/d5cy00684h

rsc.li/catalysis

## 1. Introduction

Atomically disperse catalysts, or single-atom catalysts (SACs), have gained interest due to their efficient use of precious metals and ability to facilitate reactions otherwise unfeasible on metal nanoparticles, such as rhodium SACs for hydroformylation.<sup>1</sup> Efforts to improve heterogeneous hydroformylation have focused primarily on the choice of metal oxide support. For example, isolated rhodium on tin oxide shows high selectivity and turnover frequency towards hydroformylation; however, this catalyst has a narrow operating range due to excess oxygen vacancy formation at elevated temperatures, limiting coordination accessibility of Rh centers.<sup>2</sup> Other methods to control active sites involve complicated synthesis methods, limiting their scalability; an example is the introduction of  $\text{ReO}_x$  pair-sites.<sup>3</sup> Further work has explored isolation of rhodium sites within zeolites through Rh–Zn or Rh–Co complexes.<sup>4</sup>

An intriguing aspect of SACs is the opportunity to make direct connections to design approaches typically employed for soluble organometallic catalysts. In particular, organometallic rhodium complexes have been extensively studied for hydroformylation, enabling precise control of the active site.<sup>5</sup> For example, the introduction of electron withdrawing/donating groups to diphosphine-rhodium complexes results in higher hydroformylation activity for electron deficient phosphines.<sup>6</sup> Another example is the

introduction of aromatic ligands to introduce medium-range  $\pi$ –CH interactions with the substrate – promoting a desired transition state for branched/linear aldehyde products.<sup>7,8</sup>

Inspired by molecular catalysis, one potential opportunity is to use organic surface modifiers, such as phosphonic acids (PAs), to modify the near-site environment of SACs. Work by Zakem *et al.* demonstrated that functionalization by either alkyl and fluoroalkyl phosphonic acids promotes hydroformylation, with higher PA coverages correlating to higher rates.<sup>9</sup> This work suggested that phosphonic acids impacted the activation entropy of hydroformylation, while the apparent activation enthalpy was not strongly affected. It is currently unknown whether it is possible to engineer near-surface, specific chemical interactions with organic ligands that enthalpically stabilize transition states.

Phosphonic acids have previously been used to modify the metal oxide surface<sup>10–12</sup> of supported metal nanoparticle catalysts, and to provide interfacial sites at the metal–metal oxide interface for catalytic activity.<sup>13</sup> Recent work has demonstrated the importance of functional group placement near isolated rhodium sites,<sup>14</sup> indicating potential for strong non-covalent interactions between the tail group, adsorbed species, and active sites. Benzyl phosphonic acids, specifically, were shown to modulate the activity of titania for dehydrogenation/dehydration of alcohols, with rates for dehydration being strongly correlated to the PA dipole moment.<sup>11</sup> For single atom Rh catalysts deposited on  $\text{TiO}_2$ , we expected similarly strong effects due to the close contact of the rhodium with the modified support. Therefore, here, we investigated the impact of functionalized benzyl

Department of Chemical & Biological Engineering, University of Colorado Boulder, Boulder, Colorado 80309, USA. E-mail: Will.Medlin@colorado.edu



phosphonic acids on the adsorption of CO and the hydroformylation of ethylene. We considered two hypotheses regarding potential mechanisms: (1) modifiers with different dipole moments may change the electrostatic binding strength of CO (as measured by Stark tuning effects seen in FTIR), with hydroformylation rates varying inversely with binding strength, and/or (2) local confinement at the active site may direct hydroformylation selectivity due to non-covalent tail-adsorbate interactions (described by CO bite angle measurements from FTIR), where more confined active sites will have limited conformational freedom to perform hydroformylation.

## 2. Methods

### 2.1. Synthesis

**2.1.1. Rh/TiO<sub>2</sub> synthesis.** Atomically disperse Rh/TiO<sub>2</sub> catalysts were synthesized by previously reported strong electrostatic adsorption methods.<sup>14,15</sup> Sifted, vacuum-dried titania (US Nano 3838, 5 nm nanopowder, 270 m<sup>2</sup> g<sup>-1</sup>) was added to ammonia/water to yield a ratio of ~3 m<sup>2</sup> surface area per mL solution at a pH of 10. The precursor, RhCl<sub>3</sub> (Sigma Aldrich, 98%) was dissolved in ammonium hydroxide (Fisher Scientific, 28–30%) at a concentration of 2 mg mL<sup>-1</sup> by sonication overnight. The precursor was then diluted to an appropriate loading to yield 0.3 wt% Rh/TiO<sub>2</sub> and added slowly by a syringe pump at 1.5 mL per hour. The catalyst was then calcined in synthetic air (20% O<sub>2</sub>/N<sub>2</sub>) at 350 °C for six hours followed by reduction at 100 °C in 20% H<sub>2</sub>/N<sub>2</sub> for two hours. Catalysts were synthesized in batches of 3.6 g and 4 batches were combined and thoroughly mixed for use in these studies.

**2.1.2. Phosphonic acid deposition.** Benzyl phosphonic acid (BnPA) (Thermo Scientific, 97%), 4-trifluoromethyl benzyl phosphonic acid (4-F<sub>3</sub>CBnPA) (Manchester Organics, 98%), 2,6-difluorobenzyl phosphonic acid (2,6-diFBnPA), 4-fluorobenzyl phosphonic acid (4-FBnPA) (Aurum Pharmatech, 98%), and 4-methoxy benzyl phosphonic acid (4-MeOBnPA) were used as received and deposited by a simple bulk deposition method as previously reported.<sup>11</sup> 4-MeOBnPA and 2,6-diFBnPA were provided by the Marder research group, with their syntheses reported elsewhere.<sup>16</sup> Phosphonic acids were dissolved at 10 mM in tetrahydrofuran, in a volume corresponding to a 3-fold excess of the expected monolayer surface density of ~3 nm<sup>-2</sup>.<sup>9,11</sup> The Rh/TiO<sub>2</sub> catalyst was then added, stirring overnight for approximately 16 hours for self-assembly to occur. Catalysts were then centrifuged, decanted, and annealed at 120 °C to form covalent attachments to the oxide surface by condensation of the phosphonate head group with surface hydroxyls. Annealed samples were then thoroughly rinsed with tetrahydrofuran to remove excess ligands.

### 2.2. Material characterization

**2.2.1. FTIR studies.** Deposition of phosphonic acids was confirmed by diffuse reflectance infrared Fourier transform spectroscopy (DRIFTS). Spectra were recorded using a

Thermo Fisher Scientific Nicolet 6700 with a Harrick Praying Mantis. A mirror background was collected over 64 scans, with a resolution of 4 cm<sup>-1</sup>. This was followed immediately by sample spectra collected over 16 scans at the same resolution.

Carbon monoxide probe molecule DRIFTS (CO-DRIFTS) was conducted in a closed, high-temperature cell attachment (Harrick). Samples were reduced *in situ* at 100 °C for 1 hour in 20% H<sub>2</sub>/Ar at a flow rate of 50 sccm, followed by purging at 200 sccm Ar for 30 minutes. Background spectra were collected under 200 sccm Ar at 30 °C, followed by dosing in 10% CO/He at 30 sccm for 30 minutes and subsequent purging in Ar at 200 sccm for 30 minutes. A series of scans were collected during dosing and purging cycles to confirm equilibrium was reached.

**2.2.2. X-ray photoelectron spectroscopy (XPS).** Relative loadings of phosphonic acids were confirmed using XPS, using the ratio of phosphorous to titanium. XPS was performed using a Kratos AxisSupra+ XPS system with an Al Kα<sub>1</sub> X-ray source. Elemental analysis was done using CasaXPS software. Charge correction was done by shifting C 1s peak locations to 285.0 eV and peak fitting done with a Tougaard background for survey scans and Shirley background for component scans.

### 2.3. Reaction measurements

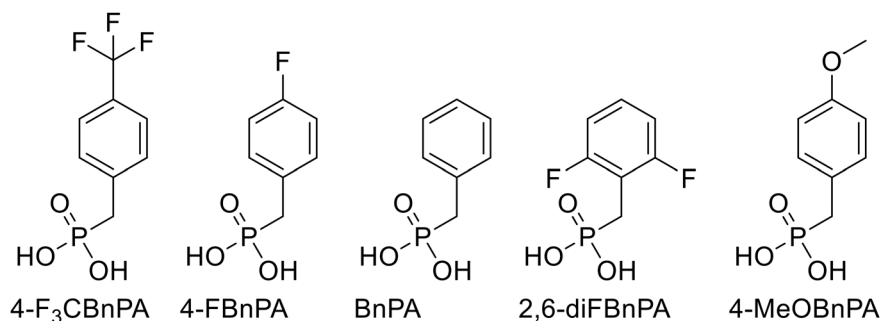
Hydroformylation activity was assessed in a stainless-steel, pressurized, gas-phase, packed-bed reactor system connected to a purge-packed Agilent 8890 GC-TCD-FID with a Hayesep D column (1/8" × 6'). All catalysts were weighed and diluted at a 1:5 ratio of catalyst:sand to ensure adequate heat transfer. Acid purified, quartz sand was used for dilution as-received (84878 Sigma-Aldrich, 40–150 mesh). Catalysts were reduced in 1:1:19 H<sub>2</sub>:CO:He at 21 sccm at 7.5 bar and 150 °C for 2 hours, then the makeup exchanged to 1:1:1:18 H<sub>2</sub>:CO:C<sub>2</sub>H<sub>4</sub>:He, maintaining 150 °C and 7.5 bar, to begin reaction measurements. The reactor outlet was sampled by the on-line GC-TCD-FID to quantify product formation rates. Turnover frequencies were calculated based on the total Rh loading on the catalyst, adjusted for the mass of deposited phosphonic acid.

## 3. Results

### 3.1. Phosphonic acid modification of Rh/TiO<sub>2</sub> confirmed spectroscopically

The 0.3 wt% Rh/TiO<sub>2</sub> catalysts were prepared as described above and modified with a series of benzyl phosphonic acids including: BnPA, 4-F<sub>3</sub>CBnPA, 2,6-diFBnPA, 4-FBnPA, and 4-MeOBnPA (Shown in Scheme 1). Ligand deposition was confirmed by the identification of specific features in DRIFTS. The expected C–H stretching modes were observed for all modified catalysts in the 2800–3100 cm<sup>-1</sup> range, attributed to the methylene spacer (2920–2980 cm<sup>-1</sup>) and C–H ring stretches (3000–3100 cm<sup>-1</sup>). All phosphonic acids exhibited C–C stretches for the aromatic ring in the 1500





**Scheme 1** Ligands used in this study, from left to right: 4-trifluoromethyl benzyl phosphonic acid (4-F<sub>3</sub>CBnPA), 4-fluorobenzyl phosphonic acid (4-FBnPA), benzyl phosphonic acid (BnPA), 2,6-difluorobenzyl phosphonic acid (2,6-diFBnPA), and 4-methoxy benzyl phosphonic acid (4-MeOBnPA).

cm<sup>-1</sup> range.<sup>11</sup> Spectra and specific peak assignments are shown in the SI (Fig. S1, Table S1).

XPS was used to compare relative loadings of phosphonic acids deposited on Rh/TiO<sub>2</sub> catalyst. Ratios of phosphorous to titanium peak areas are shown in Fig. S2. Similar surface loadings of phosphorous were observed across the studied phosphonic acids, limiting activity impacts due to coverage differences, which have previously been reported to be important.<sup>9</sup> No significant shifts in binding energy were observed between samples for P 2p and Ti 2p regions. Signal intensities for Rh were too low to enable analysis of oxidation state or loading by XPS. Further XPS analysis and spectra are shown in Fig. S3–S5 and Table S2.

### 3.2. Characterization of single-atom sites by CO-probe infrared spectroscopy

Catalysts were characterized with CO DRIFTS to verify that the single atom character of the catalysts was maintained after functionalization with PAs. Symmetric and asymmetric stretching peaks for adsorbed CO appearing at approximately 2090 cm<sup>-1</sup> and 2020 cm<sup>-1</sup> have been reported as unique to the symmetric and asymmetric gem-dicarbonyl modes,

respectively, of isolated rhodium sites.<sup>15,17–19</sup> This is consistent with previous studies confirming primarily single-atom sites, using the same synthesis method, using CO DRIFTS and a variety of characterization techniques including X-ray absorption spectroscopy and high-resolution electron microscopy.<sup>3,14,20</sup> The absence of peaks associated with CO adsorption on Rh clusters in either a linear mode at 2060 cm<sup>-1</sup> or a bridge-bound mode at 1900 cm<sup>-1</sup> indicated the absence of Rh–Rh sites (nanoparticles) at the DRIFTS detection limit. The raw spectra are shown in Fig. 1a. Notably, all modified catalysts showed 85–95% reduction in CO stretching intensity when compared to the unmodified catalyst. This is consistent with adsorption site perturbation by phosphonic acid binding observed by Zakem *et al.*, where less than 10% site accessibility was reported by CO pulse chemisorption at a monolayer of n-octyl phosphonic acid.<sup>9</sup>

Analysis of the adsorbed CO spectra across the different catalysts revealed a correlation between peak frequency and the estimated dipole moment of the SAM modifier. Fig. 1b shows the peak positions of the di-carbonyl doublet plotted against the dipole of the free phosphonic acid. The dipole sign convention is that positive is towards the phosphonic acid group (*i.e.*, toward the surface) while negative is away.

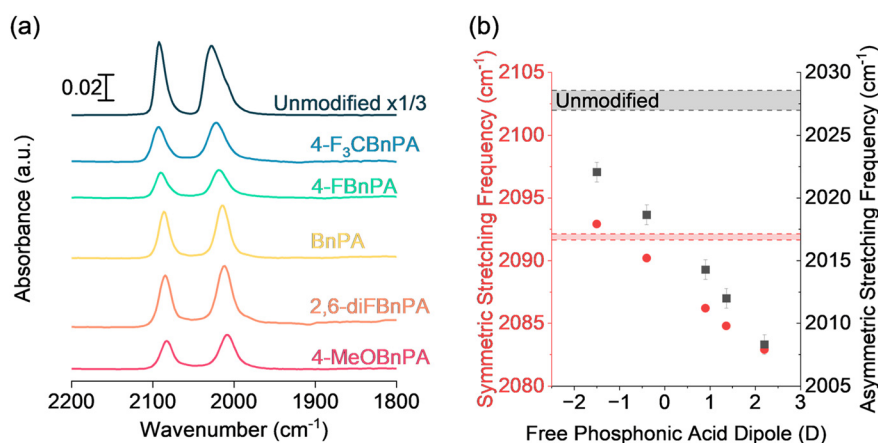


**Fig. 1** (a) DRIFT spectra for adsorbed CO on unmodified 0.3 wt% Rh/TiO<sub>2</sub> and PA-coated 0.3 wt% Rh/TiO<sub>2</sub>. (b) CO stretching frequency for left spectra plotted against the free phosphonic acid dipole.



**Table 1** CO bite angle for modified Rh/TiO<sub>2</sub> catalysts, labeled by modifier

Modifier	CO bite angle, $2\alpha$ (°)
BnPA	$99.5 \pm 0.7$
2,6-diFBnPA	$101.4 \pm 0.8$
4-FBnPA	$101.7 \pm 0.8$
4-F <sub>3</sub> CBnPA	$102.0 \pm 0.8$
4-MeOBnPA	$103.6 \pm 0.8$
Unmodified	$105.4 \pm 0.8$

Due to the symmetry of the substituted benzyl phosphonic acids, the absolute dipole was used, avoiding the need to make assumptions about phosphonic acid orientation to determine the surface-normal component. The dipole values used were previously reported from Bader charge analysis,<sup>11</sup> with dipole estimates interpolated from reported substituted benzene dipole moments for 4-MeOBnPA and 4-F<sub>3</sub>CBnPA (ref. 21) using the methodology reported in the SI (Fig. S6). This indicates that the CO stretching frequency is correlated with the molecular dipole moment. CO stretching frequency is often correlated to CO binding strength, where decreased stretching frequency indicates more strongly bound CO.<sup>3</sup>

These tuning effects are expected to be limited to electrostatic interactions of the tail with the adsorbate, due to the insulative methylene spacer on the substituted benzyl phosphonic acids. By Bader charge analysis, this spacer was shown to limit the changes to the phosphonate head group in the bound and free state.<sup>11</sup> This would limit the through-support and direct Rh–O–P interactions that vary between modifiers.

Beyond Stark tuning effects, CO-DRIFTS also provides information about the local geometry of the active site, described by the bite angle ( $2\alpha$ ) of bound CO on isolated rhodium sites. This was calculated using the ratio of asymmetric and symmetric stretching peak areas, as shown in eqn (1).<sup>22</sup>

$$\frac{A_{\text{asym}}}{A_{\text{sym}}} = \tan^2 \alpha \quad (1)$$

Calculated bite angle values are compiled in Table 1. Notably, the bite angle for the unmodified surface is the highest, and the various PA coatings decrease the bite angle to different extents. A larger bite angle can be interpreted as a proxy for a less confined active site, enabling greater mobility and flexibility of adsorbed species. The bite angles for the functionalized catalysts are somewhat higher than those reported for hydroformylation-active Rh/ZnO catalysts (94–96°).<sup>1</sup> The difference in bite angle compared to Rh/ZnO may be attributed to the use of titania as a support.

### 3.3. Influence of support modification on ethylene hydroformylation and hydrogenation

Prepared catalysts were tested under hydroformylation conditions, as described above. Ethylene and propanal were the only products detected under these conditions. Hydroformylation and hydrogenation activities were calculated as turnover frequency based on the total Rh loading. Note that this may underreport the true turnover frequency since not all sites may be accessible, especially for PA-modified catalysts. Representative time-on-stream activities are shown in Fig. 2.

For ethylene hydrogenation (Fig. 2a), the uncoated catalyst showed deactivation throughout the course of the experiment, though the rate of deactivation was highest initially. In contrast, all PA-modified catalysts showed an activation period over the initial ~5 hours, which was followed by a gradual loss in activity between hours 5 and 20. Following the initial, rapid changes in activity with time on stream, the coated and uncoated catalysts appeared to lose ethane formation activity at similarly low rates. For example, 4-MeOBnPA modified catalyst lost ~7% activity between hours 10 and 20 on stream while unmodified lost ~15%. Deactivation towards ethane has been reported previously for

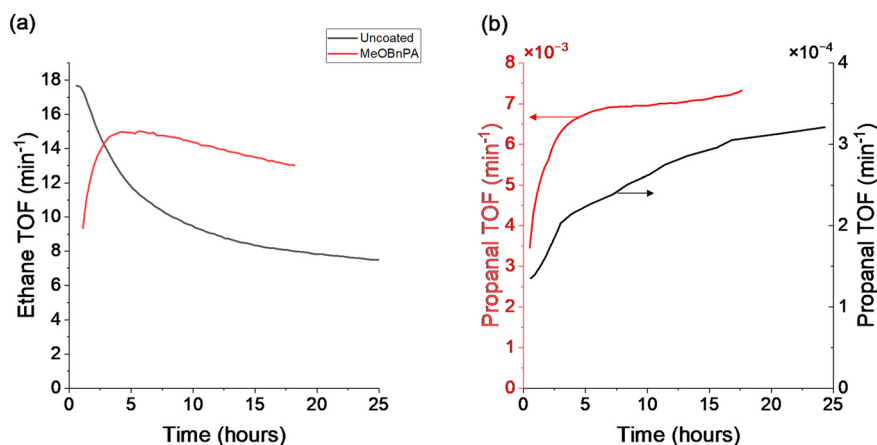


**Fig. 2** Time-on-stream plots for 4-MeOBnPA modified and uncoated Rh/TiO<sub>2</sub> catalysts under hydroformylation conditions. (a) Ethane production rate, (b) propanal production rate.





isolated Rh on  $\text{Al}_2\text{O}_3$  due to the accumulation of aldehydes strongly adsorbed to the surface.<sup>9</sup> This is expected to be similar for anatase titania supports, due to accumulation of aldehydes on the surface during the break-in period and formation of condensation products or coking,<sup>23</sup> where modified catalysts inhibit coking effects and product adsorption.

The time-on-stream behavior for hydroformylation showed different trends, with an increase in activity over time for both the uncoated and coated catalysts. The dynamics differed for coated *versus* uncoated catalysts. As shown in Fig. 2b, the uncoated catalyst exhibited a slower rise in hydroformylation activity. This is due to the previously mentioned adsorption of products to the metal oxide surface, where apparent turnover frequency is obscured until the metal oxide is fully coked.<sup>9</sup> The shorter break-in time required for modified catalysts is consistent with the need for the catalyst to activate by desorbing bound CO and adsorb ethylene to enter the hydroformylation cycle, shown in Scheme 2. This has been reported previously in homogenous systems through FTIR studies.<sup>24</sup> All modified catalysts showed similar break in times, shown in Fig. S7.

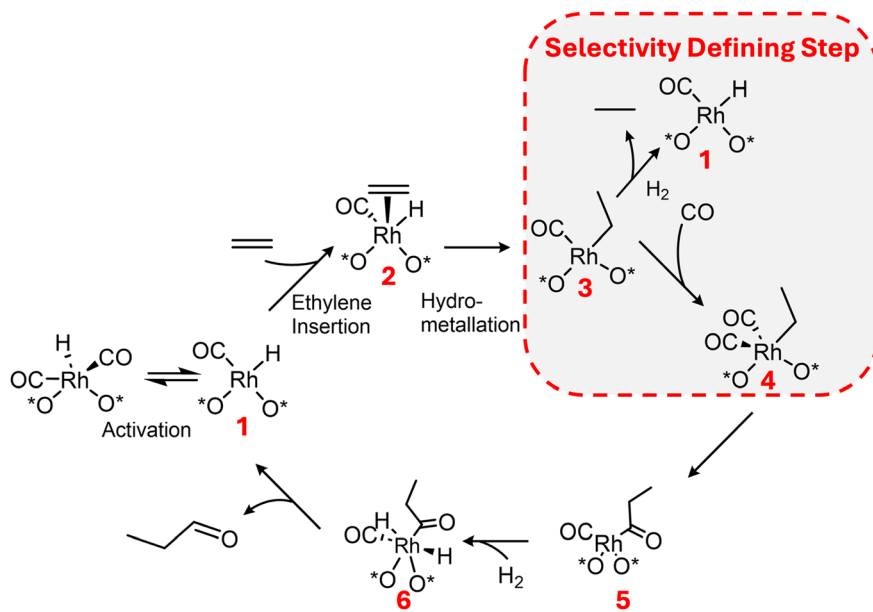
Notably, all modified catalysts showed hydroformylation rates that were approximately an order of magnitude higher than on the uncoated catalyst, shown in Fig. 2b. In contrast, while ethane formation rates showed different behavior as a function of time on stream, the apparent rates were on the same scale at all times investigated. This indicates, as reported previously, that PA coatings selectively promote hydroformylation, likely through their effect on CO adsorption and reactivity.<sup>9</sup>

We next sought to evaluate possible descriptors for hydroformylation rates on the differently functionalized

catalysts. Reaction rates were quantified for the various coated catalysts by using the average from three GC injections collected after 4 hours on stream. We found that this approach led to measured rates that varied by <5% across the injections. Moreover, given the similar time on stream behavior of the various PA-functionalized catalysts, trends in rate across catalysts were largely insensitive to other means of computing rates, such as computing them at different times on stream. Measured turnover frequencies and propanal selectivity are summarized in Table S3.

We first tested the CO symmetric stretching frequency (as measured during CO DRIFTS, Fig. 1) as a parameter predicting hydroformylation activity, hypothesizing that activity may be governed by the strength of the Rh–CO interaction. Ethylene hydrogenation and hydroformylation rates, plotted against the symmetric stretching frequency, are shown in Fig. 3. The ethylene hydrogenation activity showed a weak correlation with the position of the CO stretching frequency. However, hydroformylation rates did not show a clear trend with CO stretching frequency, suggesting that it is not an effective descriptor for catalyst performance. This shows that the aldehyde production rate does not correlate solely to electronic changes impacting CO binding strength, as expected by Stark tuning effects observed in CO-DRIFTS, and reported previously for Rh– $\text{ReO}_x$  catalysts.<sup>3</sup>

Phosphonic acids are known to deposit and covalently attach primarily to metal oxides of supported catalysts; however, the isolated rhodium sites in this case are likely to be obstructed as well, as noted earlier on CO DRIFTS peak intensities. Without quantitative analysis of the available sites after deposition, it is hard to differentiate changes in rate due to site blocking/deactivation. To mitigate this issue, the facile hydrogenation of ethylene to ethane was used as a



**Scheme 2** Adapted ethylene hydroformylation mechanism for isolated rhodium on metal oxide. O\* represent oxygen from the support. Most steps are considered reversible, but shown here as unidirectional for clarity.



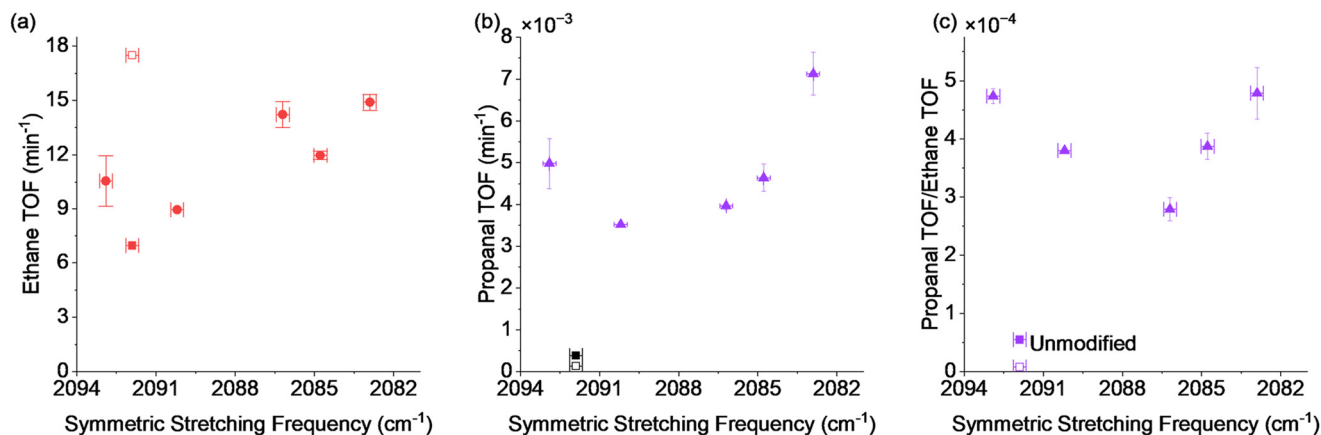


Fig. 3 (a) Ethane turnover frequency, (b) propanal turnover frequency (c) relative propanal turnover frequency to ethane turnover frequency plotted against symmetric stretching frequency from CO-DRIFTS. Uncoated catalyst rates are represented by open and closed squares for initial and final rates, respectively.

proxy for site availability. Then, the ratio of propanal and ethane formation rates was calculated and plotted against the stretching frequency in Fig. 3c. This provides a direct measure of the selectivity for hydroformylation compared to hydrogenation, which may be a better indicator of activity on a per-available-site basis. Similar to absolute activities, there is no clear correlation between the relative hydroformylation rate and the CO stretching frequency. Again, this shows that the nature of bound CO is not directly related to hydroformylation activity.

Site geometry differences related to adsorbate-tail interactions or local confinement may be important in controlling activity.<sup>14</sup> To further describe the impact of steric changes to the hydroformylation activity, the bite angle of bound CO can be used. In Fig. 4, the relative rate of propanal formation is plotted against the bite angle determined from CO-DRIFTS at 30 °C. This figure shows a strong correlation for modified catalysts, where the relative rate increases with bite angle. Note that the bite angle correlation does not extend to the uncoated catalyst, which is perhaps not surprising given the more drastic change in surface environment around the Rh center when comparing modified and unmodified materials. The PA-coated catalysts were all modified by a monolayer of (substituted) benzyl-terminated ligands, hypothetically producing relatively uniform active site environments that are subtly perturbed by the substitution of the benzyl ligand, whereas the active site without modification would be expected to lack similar steric and Rh–O–P interactions.<sup>14</sup> Ellis *et al.* made similar observations that structure–activity relations developed for closely related SAM-modified catalysts could not readily be extended to different surface environments, such as SAMs that generated different surface coverages, or to uncoated materials.<sup>11</sup>

We also tested catalyst performance at higher temperatures. We found that samples exposed to hydroformylation conditions at temperatures greater than 160 °C showed rapid deactivation towards hydroformylation,

indicating sintering. This was confirmed by post-reaction CO-DRIFTS, shown in Fig. S8. While previous work demonstrates that phosphonic acid monolayers can reduce sintering by restricting surface mobility,<sup>15</sup> hydroformylation conditions are notably harsher due to increased partial pressure of CO and H<sub>2</sub>, resulting in significant sintering even at moderate temperatures.<sup>2</sup>

## 4. Discussion

Modification of the Rh/TiO<sub>2</sub> catalysts with various PAs appeared to affect their surface chemistry in several ways. For

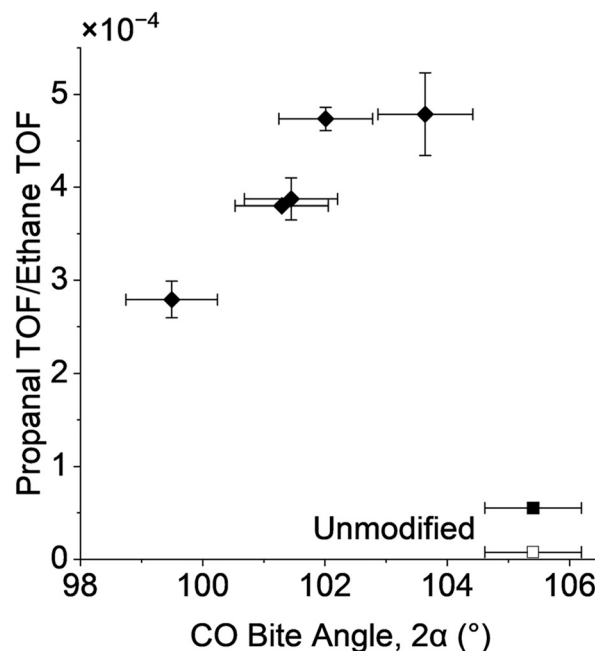


Fig. 4 Relative rate of propanal formation to ethane formation plotted against the bite angle of bound carbon monoxide calculated from CO-DRIFTS. Hollow and filled squares represent initial and final activity for the unmodified catalyst, respectively.



The adsorption of CO after hydrometallation is required for hydroformylation to occur, resulting in a relatively bulky transition state (species **4** in Scheme 2). This step is directly related to hydroformylation selectivity, as the hydrometallated species (**3**) can be readily reduced to form ethane – exiting the catalytic cycle before CO insertion. With increasing bite angle, there may be higher flexibility of the transition state to adsorb CO after hydrometallation of the

Supplementary Information available: Catalyst characterization, methods for estimating surface dipoles, and supplemental analyses of catalyst activity. See DOI: <https://doi.org/10.1039/D5CY00684H>

Some of the data supporting this article are in the SI. Complete datasets will be placed on the CU Scholar repository at <https://scholar.colorado.edu>.

## Acknowledgements

This work was supported by the Department of Energy Office of Science, Basic Energy Sciences Program, Chemical Sciences, Geosciences, and Biosciences Division (Grant DE-SC-0005239).

## References

- 1 R. Lang, T. Li, D. Matsumura, S. Miao, Y. Ren, Y.-T. Cui, Y. Tan, B. Qiao, L. Li, A. Wang, X. Wang and T. Zhang, Hydroformylation of Olefins by a Rhodium Single-Atom Catalyst with Activity Comparable to  $\text{RhCl}(\text{PPh}_3)_3$ , *Angew. Chem., Int. Ed.*, 2016, **55**(52), 16054–16058, DOI: [10.1002/anie.201607885](https://doi.org/10.1002/anie.201607885).
- 2 M. G. Farpón, W. Henao, P. N. Plessow, E. Andrés, R. Arenal, C. Marini, G. Agostini, F. Studt and G. Prieto, Rhodium Single-Atom Catalyst Design through Oxide Support Modulation for Selective Gas-Phase Ethylene Hydroformylation, *Angew. Chem., Int. Ed.*, 2023, **62**(1), e202214048, DOI: [10.1002/anie.202214048](https://doi.org/10.1002/anie.202214048).
- 3 I. Ro, M. Xu, G. W. Graham, X. Pan and P. Christopher, Synthesis of Heteroatom Rh–ReOx Atomically Dispersed Species on  $\text{Al}_2\text{O}_3$  and Their Tunable Catalytic Reactivity in Ethylene Hydroformylation, *ACS Catal.*, 2019, **9**(12), 10899–10912, DOI: [10.1021/acscatal.9b02111](https://doi.org/10.1021/acscatal.9b02111).
- 4 L. Qi, S. Das, Y. Zhang, D. Nozik, B. C. Gates and A. T. Bell, Ethene Hydroformylation Catalyzed by Rhodium Dispersed with Zinc or Cobalt in Silanol Nests of Dealuminated Zeolite Beta, *J. Am. Chem. Soc.*, 2023, **145**(5), 2911–2929, DOI: [10.1021/jacs.2c11075](https://doi.org/10.1021/jacs.2c11075).
- 5 R. Franke, D. Selent and A. Börner, Applied Hydroformylation, *Chem. Rev.*, 2012, **112**(11), 5675–5732, DOI: [10.1021/cr3001803](https://doi.org/10.1021/cr3001803).
- 6 L. A. van der Veen, M. D. K. Boele, F. R. Bregman, P. C. J. Kamer, P. W. N. M. van Leeuwen, K. Goubitz, J. Fraanje, H. Schenk and C. Bo, Electronic Effect on Rhodium Diphosphine Catalyzed Hydroformylation: The Bite Angle Effect Reconsidered, *J. Am. Chem. Soc.*, 1998, **120**(45), 11616–11626, DOI: [10.1021/ja981969e](https://doi.org/10.1021/ja981969e).
- 7 M. Kumar, R. V. Chaudhari, B. Subramaniam and T. A. Jackson, Ligand Effects on the Regioselectivity of Rhodium-Catalyzed Hydroformylation: Density Functional Calculations Illuminate the Role of Long-Range Noncovalent Interactions, *Organometallics*, 2014, **33**(16), 4183–4191, DOI: [10.1021/om500196g](https://doi.org/10.1021/om500196g).
- 8 P. Dingwall, J. A. Fuentes, L. E. Crawford, A. M. Z. Slawin, M. Bühl and M. L. Clarke, Understanding a Hydroformylation Catalyst That Produces Branched Aldehydes from Alkyl Alkenes, *J. Am. Chem. Soc.*, 2017, **139**(44), 15921–15932, DOI: [10.1021/jacs.7b09164](https://doi.org/10.1021/jacs.7b09164).
- 9 G. Zakem, I. Ro, J. Finzel and P. Christopher, Support Functionalization as an Approach for Modifying Activation Entropies of Catalytic Reactions on Atomically Dispersed Metal Sites, *J. Catal.*, 2021, **404**, 883–896, DOI: [10.1016/j.jcat.2021.07.030](https://doi.org/10.1016/j.jcat.2021.07.030).
- 10 J. Ballesteros-Soberanas, L. D. Ellis and J. W. Medlin, Effects of Phosphonic Acid Monolayers on the Dehydration Mechanism of Aliphatic Alcohols on  $\text{TiO}_2$ , *ACS Catal.*, 2019, **9**(9), 7808–7816, DOI: [10.1021/acscatal.9b02082](https://doi.org/10.1021/acscatal.9b02082).
- 11 L. D. Ellis, R. M. Trottier, C. B. Musgrave, D. K. Schwartz and J. W. Medlin, Controlling the Surface Reactivity of Titania via Electronic Tuning of Self-Assembled Monolayers, *ACS Catal.*, 2017, **7**(12), 8351–8357, DOI: [10.1021/acscatal.7b02789](https://doi.org/10.1021/acscatal.7b02789).
- 12 L. D. Ellis, J. Ballesteros-Soberanas, D. K. Schwartz and J. W. Medlin, Effects of Metal Oxide Surface Doping with Phosphonic Acid Monolayers on Alcohol Dehydration Activity and Selectivity, *Appl. Catal., A*, 2019, **571**, 102–106, DOI: [10.1016/j.apcata.2018.12.009](https://doi.org/10.1016/j.apcata.2018.12.009).
- 13 J. Zhang, L. D. Ellis, B. Wang, M. J. Dzara, C. Sievers, S. Pylypenko, E. Nikolla and J. W. Medlin, Control of Interfacial Acid–Metal Catalysis with Organic Monolayers, *Nat. Catal.*, 2018, **1**(2), 148–155, DOI: [10.1038/s41929-017-0019-8](https://doi.org/10.1038/s41929-017-0019-8).
- 14 A. H. Jenkins, E. E. Dunphy, M. F. Toney, C. B. Musgrave and J. W. Medlin, Tailoring the Near-Surface Environment of Rh Single-Atom Catalysts for Selective  $\text{CO}_2$  Hydrogenation, *ACS Catal.*, 2023, **13**(23), 15340–15350, DOI: [10.1021/acscatal.3c03768](https://doi.org/10.1021/acscatal.3c03768).
- 15 J. Zhang, C. Asokan, G. Zakem, P. Christopher and J. W. Medlin, Enhancing Sintering Resistance of Atomically Dispersed Catalysts in Reducing Environments with Organic Monolayers, *Green Energy Environ.*, 2022, **7**(6), 1263–1269, DOI: [10.1016/j.gee.2021.01.022](https://doi.org/10.1016/j.gee.2021.01.022).
- 16 A. J. Giordano, *Altering the Work Function of Surfaces: The Influential Role of Surface Modifiers for Tuning Properties of Metals and Transparent Conducting Oxides*, Georgia Institute of Technology, 2014, <https://hdl.handle.net/1853/53989> (accessed 2025-02-17).
- 17 M. J. Hülsey, B. Zhang, Z. Ma, H. Asakura, D. A. Do, W. Chen, T. Tanaka, P. Zhang, Z. Wu and N. Yan, In Situ Spectroscopy-Guided Engineering of Rhodium Single-Atom Catalysts for CO Oxidation, *Nat. Commun.*, 2019, **10**(1), 1330, DOI: [10.1038/s41467-019-09188-9](https://doi.org/10.1038/s41467-019-09188-9).
- 18 F. Doherty and B. R. Goldsmith, Rhodium Single-Atom Catalysts on Titania for Reverse Water Gas Shift Reaction Explored by First Principles Mechanistic Analysis and Compared to Nanoclusters, *ChemCatChem*, 2021, **13**(13), 3155–3164, DOI: [10.1002/cctc.202100292](https://doi.org/10.1002/cctc.202100292).
- 19 J. C. Matsubu, V. N. Yang and P. Christopher, Isolated Metal Active Site Concentration and Stability Control Catalytic  $\text{CO}_2$  Reduction Selectivity, *J. Am. Chem. Soc.*, 2015, **137**(8), 3076–3084, DOI: [10.1021/ja5128133](https://doi.org/10.1021/ja5128133).
- 20 Y. Tang, C. Asokan, M. Xu, G. W. Graham, X. Pan, P. Christopher, J. Li and P. Sautet, Rh Single Atoms on  $\text{TiO}_2$  Dynamically Respond to Reaction Conditions by Adapting Their Site, *Nat. Commun.*, 2019, **10**(1), 4488, DOI: [10.1038/s41467-019-12461-6](https://doi.org/10.1038/s41467-019-12461-6).
- 21 Benzenes, <https://www.stenutz.eu/chem/set4.php>, (accessed 2025-02-03).





- 22 J. T. Yates Jr, T. M. Duncan, S. D. Worley and R. W. Vaughan, Infrared Spectra of Chemisorbed CO on Rh, *J. Chem. Phys.*, 1979, **70**(3), 1219–1224, DOI: [10.1063/1.437603](#).
- 23 B. E. Oliphant, M. Rasmussen, L. P. Herrera, M. B. Griffin and J. W. Medlin, Aldol Condensation of Mixed Oxygenates on TiO<sub>2</sub>, *Catal. Sci. Technol.*, 2024, **14**(7), 1911–1922, DOI: [10.1039/D3CY01798B](#).
- 24 A. Jörke, A. Seidel-Morgenstern and C. Hamel, Rhodium-BiPhePhos Catalyzed Hydroformylation Studied by Operando FTIR Spectroscopy: Catalyst Activation and Rate Determining Step, *J. Mol. Catal. A:Chem.*, 2017, **426**, 10–14, DOI: [10.1016/j.molcata.2016.10.028](#).
- 25 D. Bhattacharyya, P. E. Videla, M. Cattaneo, V. S. Batista, T. Lian and C. P. Kubiak, Vibrational Stark Shift Spectroscopy of Catalysts under the Influence of Electric Fields at Electrode–Solution Interfaces, *Chem. Sci.*, 2021, **12**(30), 10131–10149, DOI: [10.1039/D1SC01876K](#).
- 26 S. Bischoff, A. Weigt, H. Mießner and B. Lücke, Soluble and Supported Carbonylation Catalysts Derived from Rhodium-Phosphonate-Phosphane Complexes, *J. Mol. Catal. A:Chem.*, 1996, **107**(1), 339–346, DOI: [10.1016/1381-1169\(95\)00233-2](#).
- 27 R. F. Heck and D. S. Breslow, The Reaction of Cobalt Hydrotetracarbonyl with Olefins, *J. Am. Chem. Soc.*, 1961, **83**(19), 4023–4027, DOI: [10.1021/ja01480a017](#).
- 28 S. Lee, A. Patra, P. Christopher, D. G. Vlachos and S. Caratzoulas, Theoretical Study of Ethylene Hydroformylation on Atomically Dispersed Rh/Al<sub>2</sub>O<sub>3</sub> Catalysts: Reaction Mechanism and Influence of the ReOx Promoter, *ACS Catal.*, 2021, **11**(15), 9506–9518, DOI: [10.1021/acscatal.1c00705](#).

